

Synthesis of SPR Au/BiVO₄ quantum dot/rutile-TiO₂ nanorod array composites as efficient visible-light photocatalysts to convert CO₂ and mechanism insight



Qiujin Shi^a, Zhijun Li^b, Lu Chen^a, Xuliang Zhang^b, Weihua Han^c, Mingzheng Xie^{a,*}, Jianlong Yang^a, Liqiang Jing^{b,*}

^a Key Laboratory of Western China's Environmental Systems (Ministry of Education), College of Earth and Environmental Sciences, Lanzhou University, Lanzhou, 730000, China

^b Key Laboratory of Functional Inorganic Materials Chemistry (Ministry of Education), School of Chemistry and Materials Science, International Joint Research Center for Catalytic Technology, Heilongjiang University, Harbin, 150080, China

^c School of Physical Science and Technology, Lanzhou University, Lanzhou, 730000, China

ARTICLE INFO

Keywords:

BiVO₄ quantum dots
r-TiO₂ nanorod arrays
Energetic charge carrier transfer
Surface plasmonic response
CO₂ conversion

ABSTRACT

It is highly desired to develop efficient visible-light-driven BiVO₄-based nano-photocatalysts with recyclable feature by modulating photogenerated electrons and extending visible-light responses. Herein, a novel nano-composite array has been successfully fabricated by uniformly decorating BiVO₄ quantum dot (BiVO₄-QD) with an average size of ~5 nm onto rutile-TiO₂ nanorod array (RTA) through the successive ionic layer adsorption and reaction processes, and exhibited high photocatalytic activity for converting CO₂ to CO and CH₄ under visible-light irradiation. The exceptional photoactivity is mainly attributed to the greatly-enhanced charge separation and prolonged charge lifetime by effectively transferring photogenerated electrons at the elevated conduction band bottom of BiVO₄ to rutile-TiO₂ nanorods as favorable electron acceptors and transport mediums by means of surface photovoltaic technique, Mott-Schottky analyses and EIS measurements. Moreover, the photoactivity of optimized BiVO₄-QD/RTA nanocomposite is further improved after loading SPR Au nanoparticles by promoting charge separation and extending visible-light responses, about 6.5-time higher than that of BiVO₄-QD decorated anatase nanoparticle film. This work provides a feasible strategy to prepare easily reused and efficient BiVO₄-based photocatalyst, which is also applicable to other semiconductors with low CB.

1. Introduction

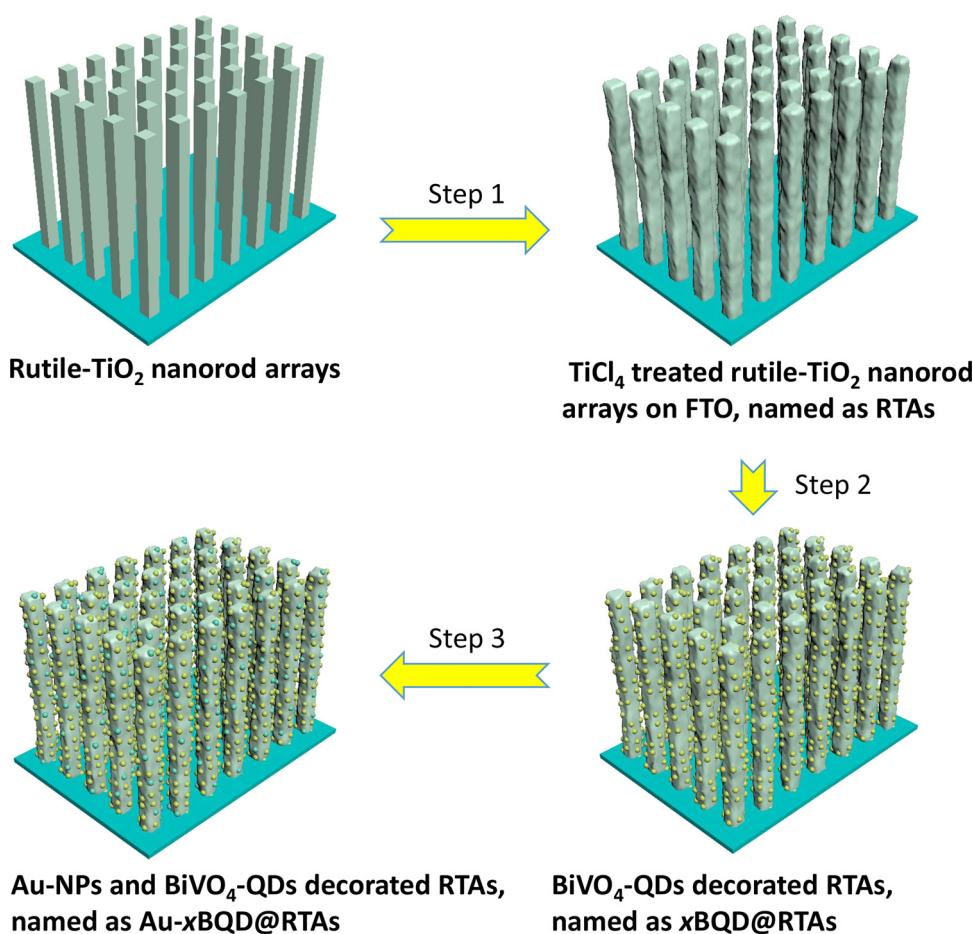
The fast growth of human population leads to sharply increased consumption of fossil fuels and enormous emission of CO₂, along with a series of environmental problems [1–3]. Photocatalytic CO₂ conversion for fuel production based on inorganic semiconductor is a promising technique to address those issues [3–6]. As the critical factor in the reaction, an ideal photocatalyst should possess good stability and appropriate energy band structures. In particular, they are narrow band-gap for wide-spectrum absorption and high conduction band (CB) level for CO₂ reduction. Among the materials reported, monoclinic bismuth vanadate (BiVO₄) meets the requirements to the greatest extent, which band-gap is ~2.4 eV and the CB is located at 0 V (vs. SHE pH = 0) [7]. Even so, it can only absorb the light with wavelength shorter than 517 nm, which accounts for 25.1% of the visible waveband of solar

spectrum, and its charge separation is still not satisfied [8]. Therefore, BiVO₄ is rarely reported as an efficient photocatalyst for CO₂ conversion. Naturally, it is highly desired to develop efficient BiVO₄-based photocatalyst by improving charge separation and extending visible-light responses.

It is well known that CO₂ reduction is harder to achieve compared with water splitting and requires the photoelectrons should be more energetic. Obviously, the CB level of BiVO₄ is not high enough since it determines the energy of photoelectrons [9]. Moreover, it is also an important limitation which leads to low charge separation rate. Generally, the band-gap of semiconductors would be widened remarkably when their size is decreased to around Bohr radius [10,11], along with an elevated CB. According to Brus Equation [12–14], the band-gap of BiVO₄ could be widened to 2.66 eV when its particle size is decreased to 5 nm (Fig. S1), and the CB is expected to be elevated remarkably

* Corresponding author.

E-mail addresses: xiemzh@lzu.edu.cn (M. Xie), jinglq@hlju.edu.cn (L. Jing).



Scheme 1. Fabrication process of Au nanoparticle and BiVO₄ quantum dot decorated rutile-TiO₂ nanorod array.

simultaneously. Therefore, it is believable that BiVO₄ with particle size of several nanometers would exhibit better performance for CO₂ conversion compared to bulk ones. However, it is challenging to obtain BiVO₄ with such a small particle size due to the fast growth rate once nucleating centers formed [15]. Fortunately, we have been obtained BiVO₄ quantum dots (BiVO₄-QDs) with a particle size around 4.7 nm in recent work through the successive ionic layer adsorption and reaction processes (SILAR) by using screw-like SnO₂ as host substrate [16]. The BiVO₄-QD/screw-like SnO₂ composite showed an improved photocatalytic activity for water splitting, and the improved activity was suggested to be mainly attributed to the elevated CB of BiVO₄. This laid the foundation for developing BiVO₄ based photocatalyst with high activity for CO₂ conversion.

Generally speaking, composite photocatalyst would show better activity compared with pristine one attributed to the enhanced charge separation resulted from the charge transfer. An ideal host substrate for BiVO₄-QD should have a CB level negative enough for CO₂ reduction and lower than that of BiVO₄-QD, thus the photoelectrons of BiVO₄-QD could be transferred without significant loss in energy. Among the numbers of materials, rutile-SnO₂ (r-SnO₂), rutile-TiO₂ (r-TiO₂) and anatase-TiO₂ (a-TiO₂) with CB levels of 0.04 V [17], -0.1 V [18–20] and -0.5 V [21,22] (vs. SHE, pH = 0) are promising candidates, in particular, r-TiO₂ may be the most promising one. As a substrate, morphology is an important factor to determine the properties. It is easy to accept that the semiconductor in nanorod form has superior electronic transmission capacity compared with that in nano-particle form [23,24]. Further, vertically-aligned nanorod array film is a favorable structure from the perspective of reutilization. Therefore, r-TiO₂ nanorod array (RTA) film is expected to be the ideal substrate for loading BiVO₄-QD.

As the prerequisite step of photocatalysis, light absorption of photocatalyst plays crucial role in determining the activity [25]. It is necessary for BiVO₄ to extend the light response since it cannot absorb the most part of the visible-light in solar spectrum, especially for the BiVO₄-QD with widened band-gap. Recently, nano-sized noble metal with surface plasmon resonance (SPR) effect attracted much attentions because it can absorb long waveband visible-light [26–28]. It is believable that the light absorption of BiVO₄-QD/r-TiO₂ nanorod array could be enhanced much by decorating SPR noble metal, such as Au nanoparticle (Au-NP). Moreover, Au-NPs loaded on the surface of photocatalyst could capture the photoelectrons, so as to promote the charge separation [28]. Therefore, it is expected that the modification of Au-NPs would further improve the photocatalytic activity of BiVO₄-QD decorated composite.

Hence, SPR Au/BiVO₄-QD/RTA nanocomposite has been fabricated through the SILAR and photochemical reduction processes. The as-prepared nanocomposite exhibits greatly enhanced activity for converting CO₂ to CO and CH₄ under visible-light irradiation. The enhanced activity is attributed to the improved charge properties and extended visible-light responses by means of surface photovoltage technique and PEC measurements. This work provides a feasible strategy to remarkably improve the performance of BiVO₄ in the reaction requires the photoelectron with high reducibility, such as CO₂ reduction and hydrogen evolution.

2. Experimental section

All reagents were of analytical grade and used without further purification.

2.1. Fabrication of BiVO_4 -QD decorated $r\text{-SnO}_2$, $r\text{-TiO}_2$ and $a\text{-TiO}_2$ films

$r\text{-SnO}_2$, $r\text{-TiO}_2$ and $a\text{-TiO}_2$ films are prepared by a doctor blade method [29] by using commercial $r\text{-SnO}_2$, $r\text{-TiO}_2$ and $a\text{-TiO}_2$ powder as raw materials and FTO as substrate and named as RSPs, RTPs and ATPs, respectively. Then, BiVO_4 -QDs were decorated on the prepared films through SILAR method [16]. In a typical process, a solution consisting of $\text{Bi}(\text{NO}_3)_4 \cdot 5\text{H}_2\text{O}$ (0.1 mmol) and ethylene glycol (100 mL) was denoted as solution A; another solution (pH = 3) consisting of NH_4VO_3 (0.1 mmol) and DI water (100 mL) was denoted as solution B. The prepared films were dipped into the solution A and B for 30 s sequentially, and every dipping in both solution A and B was recorded as 1 cycle. Every dipping was accompanied with subsequent rinsing with DI water and blow-drying. Then the treated films were annealed at 500 °C for 1 h to remove residual chemicals. Finally, the BiVO_4 -QDs were successfully decorated onto the prepared films and respectively named as $x\text{BQD@RSPs}$, $x\text{BQD@RTPs}$ and $x\text{BQD@ATPs}$, in which BQD means BiVO_4 quantum dot and x denotes the cycle number. For comparison, a film sample with a thickness of several micrometers and be made up of bulk BiVO_4 particles, was prepared by a doctor blade method [29] and named as BVO-B.

2.2. Fabrication of BiVO_4 -QD and Au-NP decorated RTA

The BiVO_4 -QD and Au-NP decorated RTA was obtained in 3 steps as diagrammed in [Scheme 1](#).

Firstly, RTAs were prepared by using a hydrothermal method reported by Aydil et al [30]. Typically, a mixture consisting of concentrated hydrochloric acid (30 mL), tetrabutyl titanate (1 mL) and deionized (DI) water (30 mL) was transferred into a Teflon-lined stainless steel autoclave after being magnetically stirred for 10 min. A piece of FTO substrate was placed into the autoclave with a 45° angle to the wall and the conductive side was facing down. The autoclave was kept at 150 °C for 20 h for the $r\text{-TiO}_2$ nanorod growth and then cooled down to room temperature. RTAs would be attained on the FTO substrate after being taken out from the autoclave, rinsed with DI water and dried in air at 60 °C for 1 h.

Secondly, to facilitate BiVO_4 -QD decoration, the as-prepared RTAs were pre-treated with 50 mM TiCl_4 at 70 °C for 0.5 h and then annealed at 500 °C for 0.5 h. Thirdly, BiVO_4 -QDs were decorated on the pre-treated RTAs through SILAR method [16] and named as $x\text{BQD@RTAs}$. The decoration amount of BiVO_4 -QD was rationally controlled by adjusting the cycle number. Finally, 1 wt% of Au-NPs were loaded on $x\text{BQD@RTAs}$ by a photochemical reduction method [28] and named as $\text{Au-}x\text{BQD@RTAs}$.

2.3. Material characterization

We characterized the microcosmic morphology with scanning electron microscope (SEM, Hitachi S-4800) and transmission electron microscope (TEM, FEI Tecnai F30). The crystal structure and surface composition were investigated with the help of X-ray diffractometer (XRD, Philips X'pert pro, Cu $\text{K}\alpha$, 0.15406 nm), micro-Raman spectrometer (JY-HR800, 532 nm laser) and X-ray photoelectron spectroscopy (XPS, Kratos-AXIS ULTRA DLD). Their optical properties were studied by spectrophotometer (TU-1901). The time-resolved surface photovoltage (TR-SPV) responses and atmosphere-controlled surface photovoltage (AC-SPV) spectra were recorded on the home-built apparatuses [31,32]. Photoelectrochemical (PEC) measurements were carried out in a quartz cell and 50 mL of 0.5 M sodium sulfate was used as electrolyte. A 500 W Xenon lamp with a cutoff filter ($\lambda > 420$ nm) was used as illumination source. The prepared composite films were used as working electrode; a platinum foil as counter electrode and a saturated KCl Ag/AgCl electrode (SSE) as reference electrode. The amplitude and applied bias during electrochemical impedance measurements were 10 mV and 1 V vs. Ag/AgCl . Incident photo-to-electron conversion efficiency (IPCE)

spectra were calculated from incident light intensity and photocurrent under 1 V vs. Ag/AgCl .

2.4. Photocatalytic activity evaluation

The photocatalytic activities of the as-prepared samples for CO_2 conversion were evaluated by means of a home-built apparatus. Typically, a piece of as-prepared film was placed into a steel reactor contained 3 mL of water and with 3.5 cm^2 area. A 300 W Xenon lamp with a 420 nm cutoff filter was used as the illumination source. Highly pure CO_2 gas was entered into the reactor for reaching ambient pressure after being passed through water. The used film was allowed to equilibrate in the $\text{CO}_2/\text{H}_2\text{O}$ system for 1 h. After being irradiated for 4 h, about 1 mL of gas produced was taken from the reaction cell for CO and CH_4 concentration analysis by means of a GC-7920 gas chromatograph (Aulight, Beijing) and a GC-2014 gas chromatograph (Shimadzu, Japan), respectively.

The photocatalytic activities of the as-prepared films for hydrogen evolution were evaluated in a LabSorlar-III-AG inline hydrogen production system (Perfect, Beijing). After being deposited with 1 wt% of Pt through an *in situ* photodeposition method [16], a piece of as-prepared film sample was placed into a mixture of DI water (90 mL) and methanol (10 mL) in the reaction cell. Prior to the reaction, O_2 and CO_2 in the mixture solution were deaerated by evacuation. A 500 W Xenon lamp with a 420 nm cutoff filter was used as cycle illumination source. The hydrogen generation rate was estimated by light irradiation time and the hydrogen concentration measured with the chromatograph equipped on LabSorlar-III-AG.

3. Results and discussion

The morphologies of the intermediate and final products have been shown in [Fig. S2](#), [Fig. 1](#) and [Fig S3a,b](#). It shows that the RSPs, RTPs and ATPs are consisted of nano-sized particles, and both of them have a thickness of $\sim 3.5\text{ }\mu\text{m}$. Meanwhile, the RTAs are consisted of ordered nanorods with diameter of 100–200 nm and length of $\sim 3\text{ }\mu\text{m}$. The nanorods are uniformly distributed on the FTO substrate and formed a continuous nanorod film. The TiCl_4 treatment makes the RTAs surface rough ([Fig. S3](#)), along with negligible changes in crystal structure and optical property. After being decorated with a certain amount of BiVO_4 -QDs, there is no observable morphology change of all the film samples. There is no quantum dot (QD) observed in the composite films, implying the size of QD is extremely small, while that of bulk BiVO_4 ranged from sub-micrometer to several micrometers ([Fig. S4](#)).

The existence of BiVO_4 -QDs and Au-NPs was evidenced by the TEM images and EDX spectra of 15BQD@RTAs and $\text{Au-}15\text{BQD@RTAs}$ shown in [Fig. 2](#). For 15BQD@RTAs , the nanorods were covered by numbers of tiny particles. The facet distance of 0.26 nm in [Fig. 2c](#) is believed from (200) plane of BiVO_4 and the 0.28 nm distance may from the (001) plane of $r\text{-TiO}_2$ [30,32,33]. It shows that BiVO_4 -QDs have a close contact with $r\text{-TiO}_2$ which may be benefited from the amorphous TiO_2 layer ($\sim 2.5\text{ nm}$) formed on the nanorod surface through TiCl_4 treatment. The size distribution of BiVO_4 -QDs is shown in [Fig. 2d](#) and it ranges from 3.25 nm to 6.25 nm, which fits the normal distribution well. Further, through a photochemical reduction process, the Au-NPs with a size of $\sim 10\text{ nm}$ were decorated on the $r\text{-TiO}_2$ nanorod in BQD@RTAs . The result of EDX analysis indicates that the Au-NP and BiVO_4 -QD decorated RTA is made up of O, Ti, Bi, V and Au. From the EDS elemental maps ([Fig. 2g](#)), the distributions of those elements in Au-BQD@RTAs are uniform.

The structural informations were provided by their XRD patterns and Raman spectra. The XRD pattern shown in [Fig. 3a](#) indicates the substrates in as-prepared composite samples are rutile- SnO_2 , rutile- TiO_2 and anatase- TiO_2 [30,34,35], respectively. The extraordinary diffraction peak at 62.9° of 15BQD@RTAs indicates the nanorod is highly oriented along [001] against the FTO substrate [36], which has been

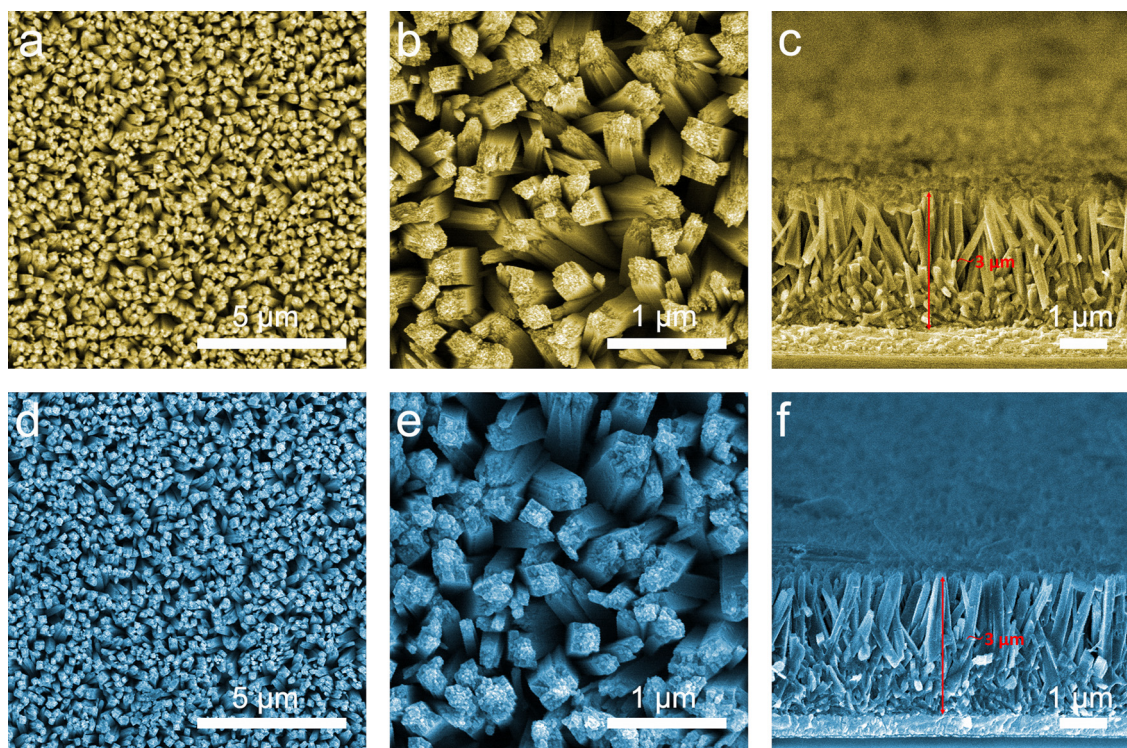


Fig. 1. Microstructure of nanorod array. (a,b) and (d,e) are plane-view SEM images of RTAs and 15BQD@RTAs at different magnifications, respectively; (c) and (f) are their cross-sectional SEM images.

observed in the SEM images. There is only a weak peak from BiVO_4 found in composite films, demonstrating the small decoration volume and low crystallinity of the BiVO_4 -QD. In addition, there is no peaks from Au found in Au-15BQD@RTAs, implying its modification volume is much smaller than that of BiVO_4 -QD. The mere existence of BiVO_4 was further verified by Raman spectra shown in Fig. 3b, in which the peak at 822 cm^{-1} assigned to BiVO_4 is nearly invisible compared with the peaks from r-TiO₂ at 448 cm^{-1} and 610 cm^{-1} and from a-TiO₂ at 395 cm^{-1} , 515 cm^{-1} and 637 cm^{-1} [37–39].

XPS measurements were carried out to study the surface chemical compositions. Fig. S5 shows the survey spectrum and high-resolution spectra of Au-15BQD@RTAs. In Fig. S5, peaks originating from Ti, O, Bi, V and Au were found, which is consistent with the EDX results. The peaks at 458.8 eV and 464.6 eV are ascribed to Ti 2p_{3/2} and 2p_{1/2} in r-TiO₂ [38], while the peaks at 159.2 eV, 164.5 eV, 517 eV and 524.6 eV are ascribed to Bi 4f_{7/2} and 4f_{5/2}, V 2p_{3/2} and 2p_{1/2} in BiVO_4 [40]. The peaks at 84 eV and 87.6 eV are ascribed to Au 4f_{7/2} and 4f_{5/2} [41]. In addition, the mole ratio of Bi/Ti is about 0.16, while that of Au/Ti is about 0.02, which is consistent with the results of XRD patterns.

The optical effects from BiVO_4 -QDs and Au-NPs were investigated by means of UV-vis absorption measurements as shown in Fig. 4 and Fig. S6. The absorption band edges of RSPs, RTPs, RTAs, ATPs and BVO-B are about 360 nm, 410 nm, 410 nm, 390 nm and 510 nm, respectively, which is consistent with the reported results [38,42,43]. After being decorated a certain amount of BiVO_4 -QDs, the samples show enhanced absorptions in visible-light region. The more BiVO_4 -QDs decorated, the high visible absorption (Fig. S6b), meaning that the enhanced visible-light absorption is attributed to BiVO_4 -QDs. The absorption band edge of BiVO_4 -QD is obviously blue-shifted compared with that of bulk BiVO_4 , it is mainly due to the band-gap widening effect resulting from the particle size reducing [44]. After being decorated with Au-NPs, the BiVO_4 -QD decorated RTA exhibits obvious absorption of light with wavelength longer than 470 nm. This enhancement is mainly attributed to the SPR effect [28]. The band-gaps of samples were determined by means of Tauc plots converted from Fig. 4a and Fig. S6b and presented

in Fig. 4b. It is clear that the band-gaps of BiVO_4 in bulk and r-TiO₂ are 2.41 eV and 3.03 eV, respectively, which are in accordance with previous reports [7,45]. After being decorated with BiVO_4 -QDs, the absorption edge of r-TiO₂ could be red-shifted to 2.62 eV. According to Lee's work and Fig. S1, it is suggested that the band-gap of BiVO_4 -QD is approximate to and a little larger than 2.62 eV [46], implying it has an elevated CB compared with bulk one. However, the widened band-gap makes BiVO_4 -QDs can only absorb the light shorter than 470 nm, which only accounts for ~9.5% of the visible waveband of solar spectrum.

SPV and PEC measurements were carried out to study the charge carrier properties. Fig. 5a,b show the SPV spectra in air, from those it is clear that RSPs, RTPs, RTAs and ATPs samples show ignorable SPV responses under the light irradiation with wavelength longer than 420 nm due to their wide band-gaps. After being decorated with BiVO_4 -QDs, the SPV responses of them in the range from 470 nm to 420 nm get enhanced. At low decoration amount, the SPV response is proportional to the amount of BiVO_4 -QDs. It began decreasing after reaching the optimized cycle number of 15. This degradation may be due to the conglomeration of excess QDs which hampered the charge transfer to electron acceptor because of the limited electron diffusion length in BiVO_4 [47,48]. However, for RSPs and ATPs, this enhancement is limited. Generally speaking, the higher the SPV response, the higher the charge carrier separation rate. It is implied that the photogenerated electrons of BiVO_4 -QDs have transferred to r-TiO₂, leading to efficient charge carrier separation. In contrast, they may could not transfer to a-TiO₂ and r-SnO₂ or be hard to be captured by O₂ after being transferred. In addition, RTAs and 15BQD@RTAs show stronger SPV responses compared with RTPs and 15BQD@RTPs, respectively, indicating improved charge carrier separations which benefit from the efficient electron transport. Moreover, the SPV response of 15BQD@RTAs is further enhanced after being decorated by Au-NPs. The SPV response under the light irradiation with wavelength longer than 470 nm is due to the SPR effect of Au [28].

Same results were found in PEC measurements under irradiation of light with wavelength longer than 420 nm (Fig. 5c and Fig. S7). During

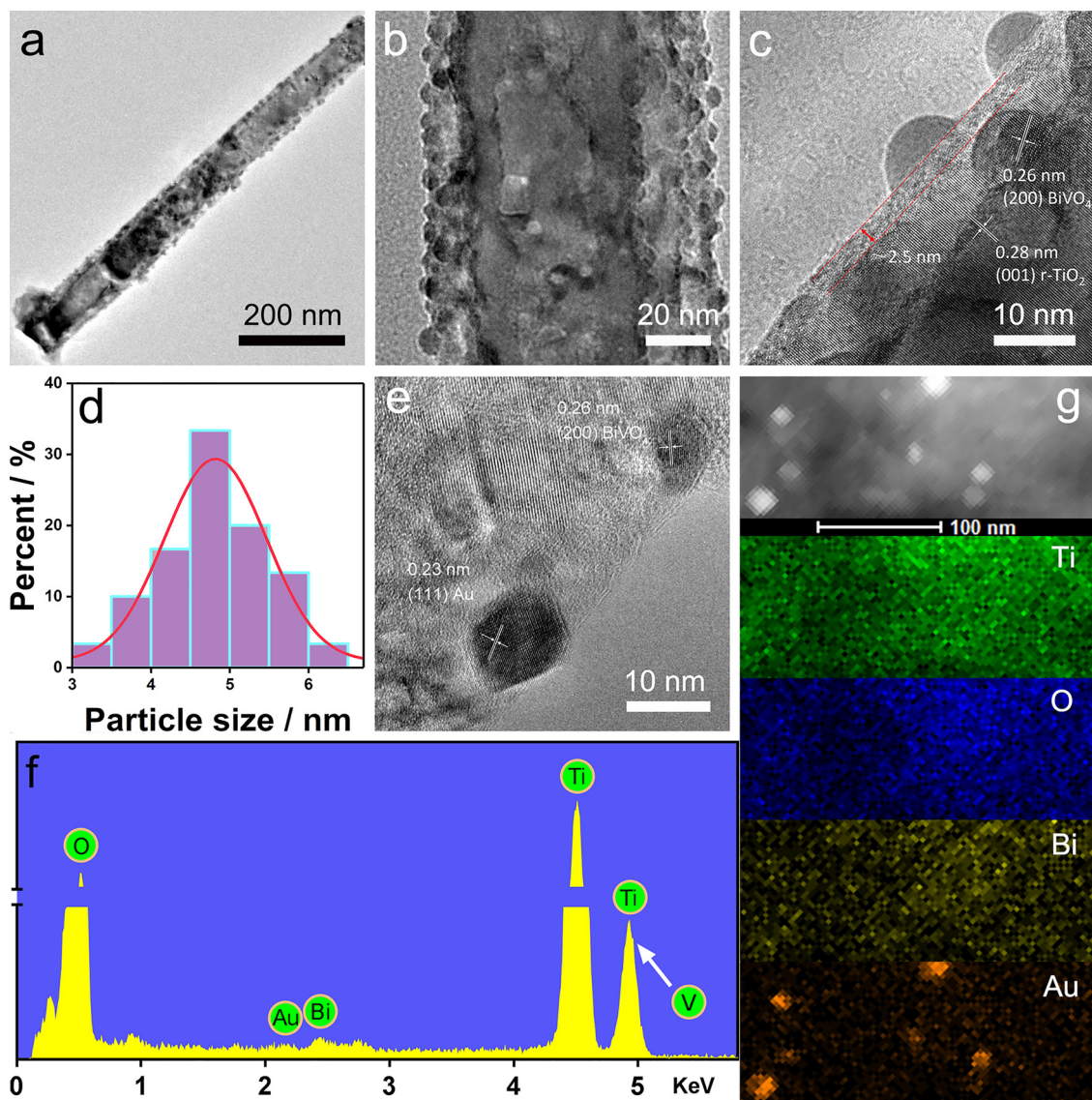


Fig. 2. Decoration of BiVO_4 quantum dots and Au nanoparticles on rutile- TiO_2 nanorod. (a), (b), (c) and (d) are TEM images of 15BQD@RTAs at different magnifications and the corresponding particle size distribution; (e), (f) and (g) are TEM image, EDX spectra and EDS elemental maps of Au-15BQD@RTAs, respectively.

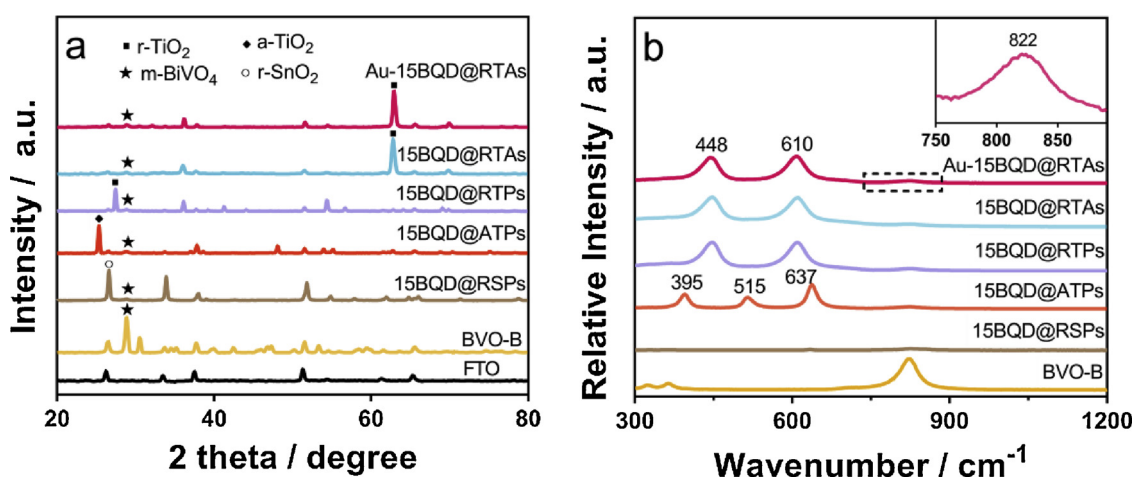


Fig. 3. Structural compositions. XRD patterns (a) and Raman spectra (b) of samples, the inset in (b) is the magnification of the rectangular area marked.

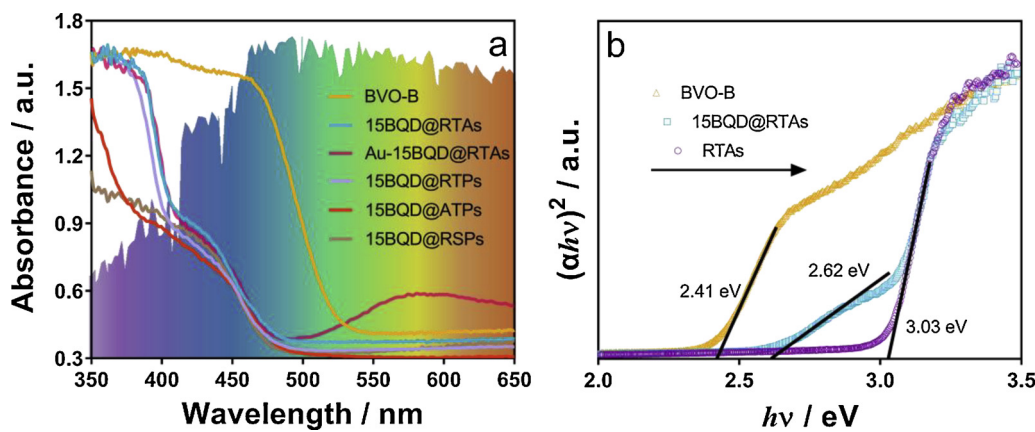


Fig. 4. Optical absorption and band-gap. (a) is the UV-vis absorption spectra, (b) is the corresponding Tauc plots.

the measurements, photogenerated electrons in working electrode (WE) would transfer to counter electrode (Pt foil) under positive bias to react with protons, resulting in a current, while the holes would react with water. Therefore, the generation of photocurrent depends on the separation of charge carriers, thus its density reflects the charge carrier separation rate. The result of long time $I-t$ measurement shown in Fig. S8 indicates that the Au-NP and BiVO₄-QD decorated RTA has good stability. As the TR-SPV responses shown in Fig. 5d, the improvement in separation of the charge is benefit from the prolonged lifetime.

CO₂ conversion under visible-light irradiation was carried out to evaluate the activities of the as-prepared samples. There is no CO or

CH₄ detected on RSPs, RTPs, RTAs and ATPs as afore predicted due to the wide band-gaps. After being decorated with BiVO₄-QDs, the activities of RTPs and RTAs are enhanced remarkably, especially for the latter (Fig. 6). Meanwhile, those of RSPs and ATPs are improved slightly. For the BiVO₄-QD decorated RTA, the photocatalytic activity tends to decrease when increase the BiVO₄ amount, and 15BQD@RTAs is much more active than others, which is similar to the results of SPV and PEC measurements. In addition, they also exhibit good performance in splitting water to hydrogen, the hydrogen generation rate can reach $1.8 \mu\text{mol}\cdot\text{cm}^{-2}\cdot\text{h}^{-1}$ over 15BQD@RTAs with the aid of Pt as co-catalyst in methanol solution under visible light irradiation (Fig. S9 and

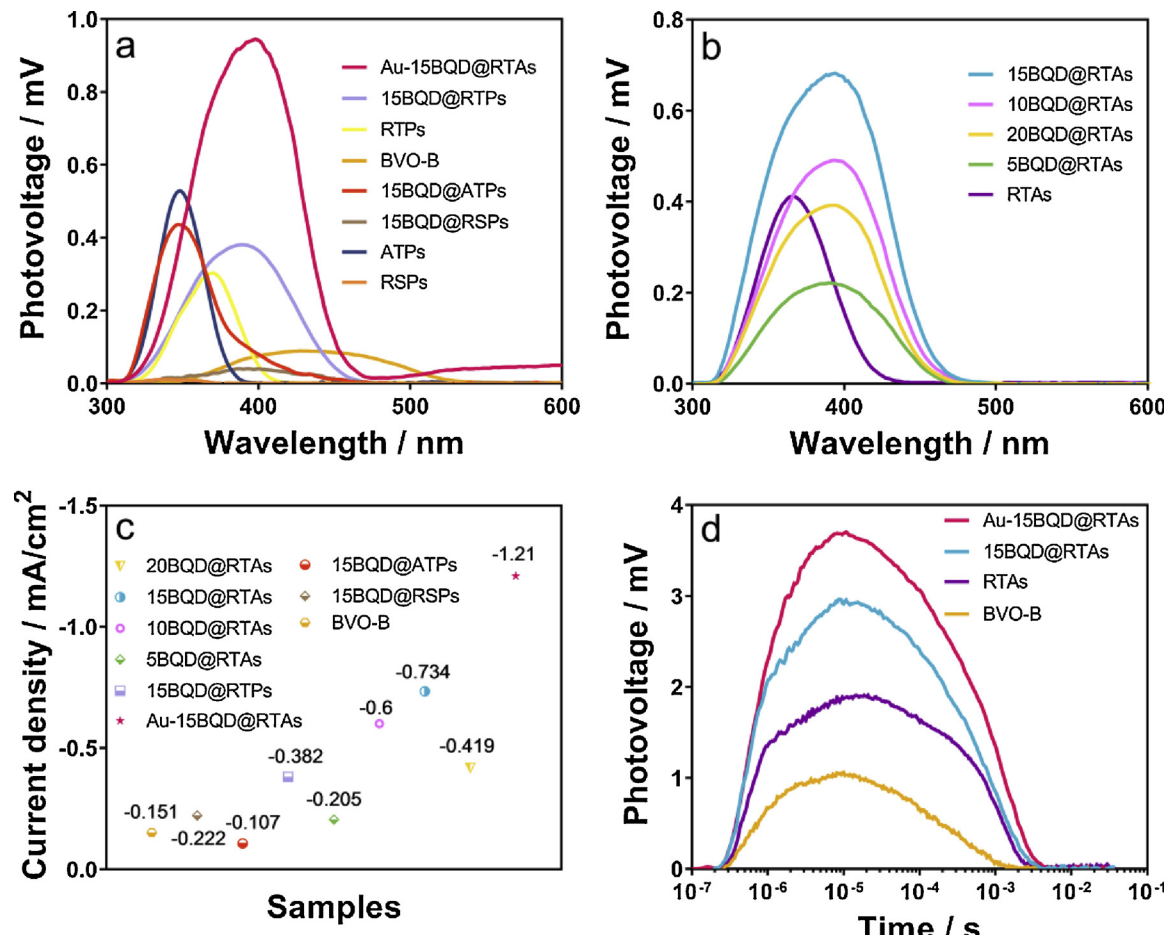
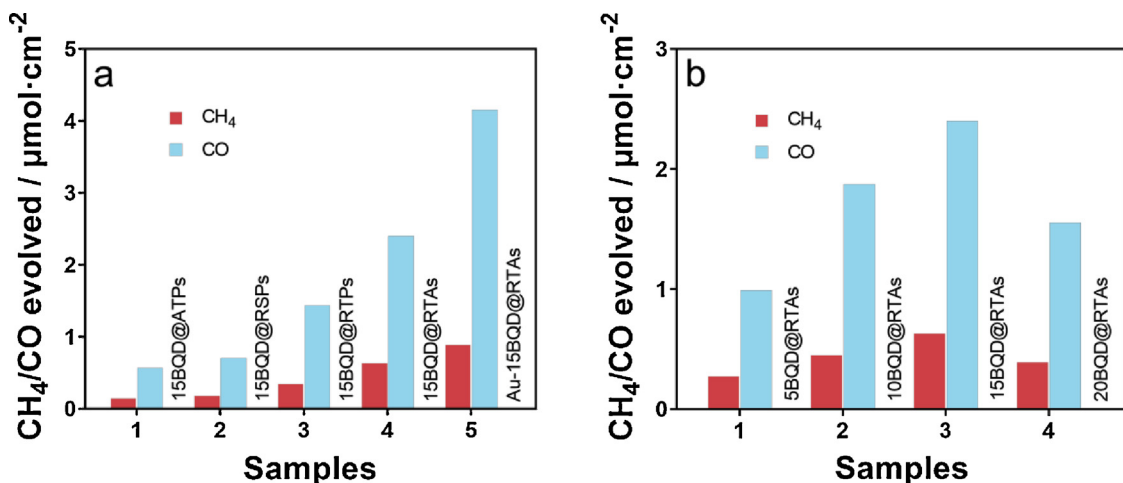


Fig. 5. Photogenerated charge properties. (a) and (b) are surface photovoltaic spectra in air; (c) is photocurrent densities under irradiation of light with wavelength longer than 420 nm; (d) is time-resolved surface photovoltaic responses in air. (c) is based on the $I-t$ curves shown in Fig. S7 in Supporting Information.

Fig. 6. CO₂ conversion under irradiation of light with wavelength longer than 420 nm.

S10). The modification of Au-NPs makes the activity of 15BQD@RTAs for CO₂ conversion enhanced further, about 6.5-time higher than that of 15BQD@ATPs, which is the composite sample with lowest activity in this work. It is noted that the activities of samples for reducing CO₂ to CH₄ is much lower than to CO, though the redox potential required for the latter is lower [49]. It is may attributed to 2 reasons. On the one hand, CH₄ production is an 8-electron process, and requires the electrons should have long lifetimes [49]. On the other hand, the CB level of r-TiO₂ is still not high enough, which determines that the photoelectrons are deficient in energy to overcome the overpotential [50]. BVO-B shows negligible activity because its CB level is not negative enough. In addition, there is no significant decrease in activity of Au-15BQD@RTAs after being reused for 5 times (Fig. S11), indicating that it has good stability, which is in good accordance with the result of long time *I-t* measurement.

The enhanced activity is believed to be attributed to the improved light absorption and charge carrier properties in such composite nanostructures. For bulk BiVO₄, the CB is located at 0 V, barely meets the requirements for CO₂ reduction and proton reduction [32,49,51]. In this work, the BiVO₄-QDs have a band-gap of ~2.62 eV, about ~0.2 eV wider than that of bulk BiVO₄, implying its CB is evaluated. According to Fig. 4, BiVO₄-QDs could be excited under the light irradiation shorter than 470 nm. Although its absorption edge is blue-shifted by ~40 nm compared to BVO-B, its electrons are more energetic and would transfer to a proper acceptor more easily. Among r-SnO₂, r-TiO₂ and a-TiO₂ studied in this work, r-TiO₂ is promising one, in particular, it is RTAs since the naorod structure is benefit for the transport of transferred electron. This spatial charge transfer from BiVO₄-QD to RTA makes the

charge lifetime be prolonged and then promotes the charge separation. Moreover, the transferred electrons would be captured by Au and thus further enhance the separation (Fig. 7). Since the CB of r-TiO₂ is expected to be just a little lower than that of BiVO₄-QD, the electrons of the latter could transfer to the former without signification energy loss. In addition, the reduced light absorption of BiVO₄-QD is recovered and further enhanced by decorating SPR Au-NPs. When the composite is irradiated by the light longer than 470 nm, the oscillating hot electrons from Au can transfer into RTAs and then take part in the reduction reaction. As a result, the Au-NP and BiVO₄-QD decorated r-TiO₂ nanorod array exhibits obviously enhanced IPCE (16.3% at the wavelength of 425 nm) (Fig. S12) and improved activity for CO₂ conversion.

The assumption is supported by the results of PEC and surface photovoltage measurements. The flat-band potentials (FBPs) of as-prepared samples are determined by means of Mott-Schottky analysis and shown in Fig. 8a and Fig. S13. For bare samples, the order of FBPs from negative to positive is: ATPs > RTPs ≈ RTAs > BVO-B ≈ RSPs. In specific electrolyte, the FBP reflects the position of Fermi level, which is very close to CB minimum for N-type semiconductor [52]. Thus, this order provides a determination of the relative locations of CB. After being decorated with BiVO₄-QDs, the FBP of ATPs is shifted to more positive, while those of the others are shifted to more negative, indicating the CB level of BiVO₄-QD is lower than a-TiO₂ and higher than r-TiO₂ and r-SnO₂. Naturally, the electrons generated in BiVO₄-QDs could be transferred to r-TiO₂ and r-SnO₂ more easily than to a-TiO₂. Therefore, 15BQD@ATPs exhibits the lowest activity, which is mainly resulted from BiVO₄-QDs. As the electron acceptor, r-TiO₂ is more promising compared with r-SnO₂, because the CB level of latter is low

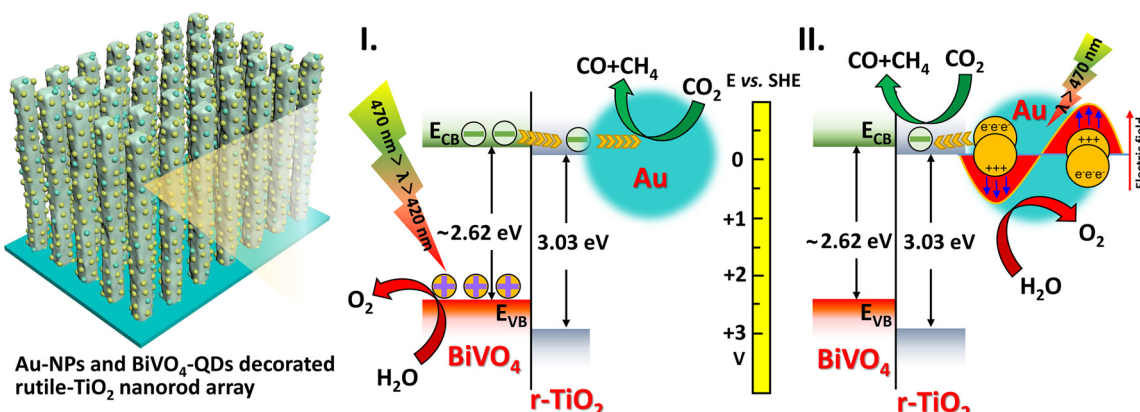


Fig. 7. Schematic of charge transfer, separation and reaction.

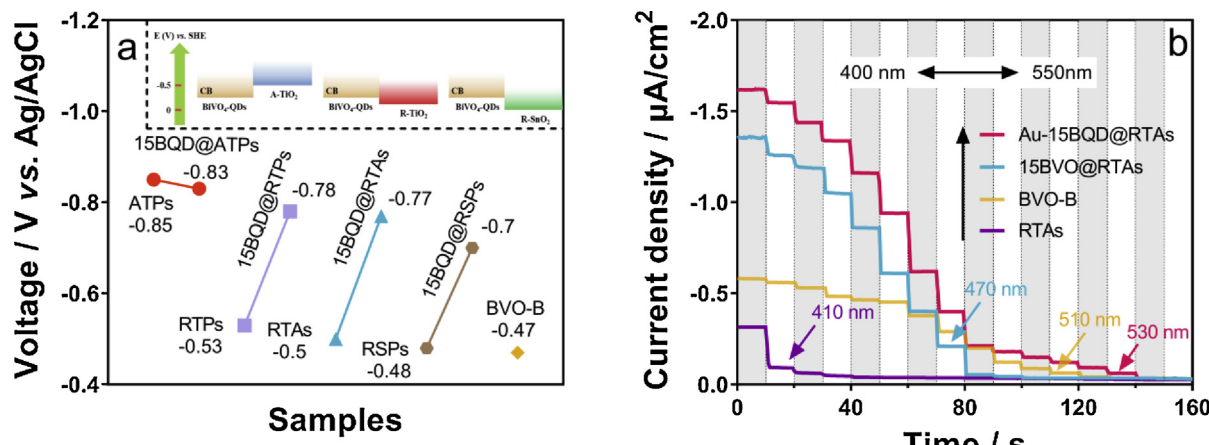


Fig. 8. Flat-band potentials (a) and photocurrent action spectra under different excitation wavelengths (b). (a) is based on the Mott-Schottky plots shown in Fig. S13 in Supporting Information. The electrolyte used is 0.5 M Na₂SO₄ and the applied bias is 1 V vs. Ag/AgCl. The inset in (a) represents the relative locations of conduction bands of materials.

and thus the transferred electrons would lose much reducibility.

Fig. S14 show the EIS Nyquist spectra, in which RTAs shows a remarkably reduced capacitive radius compared with RTPs. Generally, the radius represents the charge transfer resistance proportionally [53,54]. Therefore, it is suggested that the charge could be easily transported in RTAs, implying it is a good electron acceptor and the composite based on it would exhibit efficient PEC performance (Fig. S15). It is seen that the capacitive radius of 15BQD@RTAs is smaller than both RTAs and BVO-B, suggesting BiVO₄-QDs are in well contact with RTAs and the charge transfer between them would be unhindered [44]. Further, Au-15BQD@RTAs and 15BQD@RTAs, as well as 15BQD@RTPs, show high current densities under the irradiation of the light with wavelength corresponding to the band-gap energy of BiVO₄-QDs and characteristic absorption of Au-NPs compared with RTAs, BVO-B and others (Fig. 8b and Fig. S16), proving the charge carrier transfer indirectly. Moreover, unlike the intensity of SPV signal of pristine nano-sized semiconductor is proportional to the O₂ concentration in general [31,55], a considerable SPV signal is detected on 15BQD@RTAs and Au-RTAs in N₂ atmosphere (Fig. S17), pointing out that there are charge transfers in them [16,32].

4. Conclusions

In summary, we have successfully fabricated a high performance visible-light photocatalyst with Au-NPs, BiVO₄-QDs and RTAs. The low CB limit of BiVO₄ for CO₂ reduction has been overcome by means of band-gap widening effect of QD. Profiting from the elevated CB of BiVO₄ in QD state, the photoelectrons in BiVO₄-QDs are energetic and could be easily transferred to r-TiO₂ nanorod with low resistance, leading to prolonged charge carrier lifetime and improved separation. Moreover, the decorated Au-NPs can play multiple promoting roles under different irradiation conditions: (i) it could capture the transferred photoelectrons and thus to further promote the charge separation in waveband shorter than 470 nm; (ii) it could absorb the light with wavelength longer than 470 nm, so as to extend the visible-light responses. As a result, the as-prepared SPR Au/BiVO₄-QD/RTA nanocomposite exhibits high activity for CO₂ conversion, about 6.5-time higher than that of BiVO₄-QD decorated anatase nanoparticle film.

Acknowledgments

This work was financially supported by the National Natural Science Foundation of China (21607066; U1401245; 91622119) and the Fundamental Research Funds for the Central Universities (lzujbky-2018-142; lzujbky-2018-it84).

Appendix A. Supplementary data

Supplementary material related to this article can be found, in the online version, at doi:<https://doi.org/10.1016/j.apcatb.2018.11.089>.

References

- [1] N.J. Abram, H.V. McGregor, J.E. Tierney, M.N. Evans, N.P. McKay, D.S. Kaufman, *Nature* 536 (2016) 411–418.
- [2] T. Nakajima, Y. Tamaki, K. Ueno, E. Kato, T. Nishikawa, K. Ohkubo, Y. Yamazaki, T. Morimoto, O. Ishitani, *J. Am. Chem. Soc.* 138 (2016) 13818–13821.
- [3] F. Raziq, Y. Qu, M. Humayun, A. Zada, H. Yu, L. Jing, *Appl. Catal. B: Environ.* 201 (2017) 486–494.
- [4] R. Shi, G.I.N. Waterhouse, T. Zhang, *Sol. RRL* 1 (2017) 1700126.
- [5] X. Meng, L. Liu, S. Ouyang, H. Xu, D. Wang, N. Zhao, J. Ye, *Adv. Mater.* 28 (2016) 6781–6803.
- [6] G. Zhang, G. Liu, L. Wang, J.T.S. Irvine, *Chem. Soc. Rev.* 45 (2016) 5951–5984.
- [7] C. Jiang, S.J.A. Moniz, A. Wang, T. Zhang, J. Tang, *Chem. Soc. Rev.* 46 (2017) 4645–4660.
- [8] F. Zhou, Y. Min, J. Fan, Q. Xu, *Chem. Eng. J.* 266 (2015) 48–55.
- [9] W. Jiang, Q. Ruan, J. Xie, X. Chen, Y. Zhu, J. Tang, *Appl. Catal. B: Environ.* 236 (2018) 428–435.
- [10] M.D. Regalacio, M.-Y. Han, *Acc. Chem. Res.* 43 (2010) 621–630.
- [11] F.E. Osterloh, *Chem. Soc. Rev.* 42 (2013) 2294–2320.
- [12] K. Kočí, L. Matějová, O. Kozák, L. Čapek, V. Valeš, M. Reli, P. Praus, K. Šafářová, A. Kotarba, L. Obalová, *Appl. Catal. B: Environ.* 158–159 (2014) 410–417.
- [13] Y. Park, K.J. McDonald, K.-S. Choi, *Chem. Soc. Rev.* 42 (2013) 2321–2337.
- [14] R. Venkatesan, S. Velumani, M. Tabellout, N. Errien, A. Kassiba, *J. Phys. Chem. Solids* 74 (2013) 1695–1702.
- [15] W. Sun, M. Xie, L. Jing, Y. Luan, H. Fu, *J. Solid State Chem.* 184 (2011) 3050–3054.
- [16] M. Xie, Z. Zhang, W. Han, X. Cheng, X. Li, E. Xie, *J. Mater. Chem. A* 5 (2017) 10338–10346.
- [17] A. Zada, M. Humayun, F. Raziq, X. Zhang, Y. Qu, L. Bai, C. Qin, L. Jing, H. Fu, *Adv. Energy Mater.* 6 (2016) 1601190.
- [18] K. Maeda, *Chem. Commun.* 49 (2013) 8404–8406.
- [19] L. Li, J. Yan, T. Wang, Z.-J. Zhao, J. Zhang, J. Gong, N. Guan, *Nat. Commun.* 6 (2015) 5881.
- [20] R. Li, Y. Weng, X. Zhou, X. Wang, Y. Mi, R. Chong, H. Han, C. Li, *Energy Environ. Sci.* 8 (2015) 2377–2382.
- [21] Q.D. Truong, T.H. Le, J.-Y. Liu, C.-C. Chung, Y.-C. Ling, *Appl. Catal. A: Gen.* 437–438 (2012) 28–35.
- [22] P. Dai, G. Zhang, Y. Chen, H. Jiang, Z. Feng, Z. Lin, J. Zhan, *Chem. Commun.* 48 (2012) 3006–3008.
- [23] T. Jiang, T. Xie, L. Chen, Z. Fu, D. Wang, *Nanoscale* 5 (2013) 2938–2944.
- [24] J. Yu, Y. Wang, W. Xiao, *J. Mater. Chem. A* 1 (2013) 10727–10735.
- [25] X. Chen, C. Li, M. Grätzel, R. Kostecki, S.S. Mao, *Chem. Soc. Rev.* 41 (2012) 7909–7937.
- [26] Z. Bian, T. Tachikawa, P. Zhang, M. Fujitsuka, T. Majima, *J. Am. Chem. Soc.* 136 (2014) 458–465.
- [27] R. Shi, Y. Cao, Y. Bao, Y. Zhao, G.I.N. Waterhouse, Z. Fang, L.Z. Wu, C.H. Tung, Y. Yin, T. Zhang, *Adv. Mater.* 29 (2017) 1700803.
- [28] A. Zada, Y. Qu, S. Ali, N. Sun, H. Lu, R. Yan, X. Zhang, L. Jing, *J. Hazard. Mater.* 342 (2018) 715–723.
- [29] M. Xie, J. Bian, M. Humayun, Y. Qu, Y. Feng, L. Jing, *Chem. Commun.* 51 (2015) 2821–2823.
- [30] B. Liu, E.S. Aydil, *J. Am. Chem. Soc.* 131 (2009) 3985–3990.
- [31] L. Jing, W. Zhou, G. Tian, H. Fu, *Chem. Soc. Rev.* 42 (2013) 9509–9549.

[32] M. Xie, X. Fu, L. Jing, P. Luan, Y. Feng, H. Fu, *Adv. Energy Mater.* 4 (2014) 1300995.

[33] B. Cai, D. Zhong, Z. Yang, B. Huang, S. Miao, W.-H. Zhang, J. Qiu, C. Li, *J. Mater. Chem. C* 3 (2015) 729–733.

[34] Z. Zhang, C. Gao, Z. Wu, W. Han, Y. Wang, W. Fu, X. Li, E. Xie, *Nano Energy* 19 (2016) 318–327.

[35] M. Xie, Q. Meng, P. Luan, Y. Feng, L. Jing, *RSC Adv.* 4 (2014) 52053–52059.

[36] M. Lv, D. Zheng, M. Ye, J. Xiao, W. Guo, Y. Lai, L. Sun, C. Lin, J. Zuo, *Energy Environ. Sci.* 6 (2013) 1615–1622.

[37] J.-S. Yang, J.-J. Wu, *Nano Energy* 32 (2017) 232–240.

[38] T.-D. Nguyen-Phan, S. Luo, D. Vovchok, J. Llorca, J. Graciani, J.F. Sanz, S. Sallis, W. Xu, J. Bai, L.F.J. Piper, D.E. Polyansky, E. Fujita, S.D. Senanayake, D.J. Stacchiola, J.A. Rodriguez, *ACS Catal.* 6 (2016) 407–417.

[39] H. Khan, M.G. Rigamonti, G.S. Patience, D.C. Boffito, *Appl. Catal. B: Environ.* 226 (2018) 311–323.

[40] W. Luo, Z. Li, T. Yu, Z. Zou, *J. Phys. Chem. C* 116 (2012) 5076–5081.

[41] C. Marchal, A. Piquet, M. Behr, T. Cottineau, V. Papaefthimiou, V. Keller, V. Caps, *J. Catal.* 352 (2017) 22–34.

[42] L. Zhang, W. Yu, C. Han, J. Guo, Q. Zhang, H. Xie, Q. Shao, Z. Sun, Z. Guo, *J. Electrochem. Soc.* 164 (2017) H651–H656.

[43] S.N.F.M. Nasir, H. Ullah, M. Ebadi, A.A. Tahir, J.S. Sagu, M.A. Mat Teridi, *J. Phys. Chem. C* 121 (2017) 6218–6228.

[44] J. Yang, Q. Shi, R. Zhang, M. Xie, X. Jiang, F. Wang, X. Cheng, W. Han, *Carbon* 138 (2018) 118–124.

[45] D.O. Scanlon, C.W. Dunnill, J. Buckeridge, S.A. Shevlin, A.J. Logsdail, S.M. Woodley, C.R.A. Catlow, M.J. Powell, R.G. Palgrave, I.P. Parkin, G.W. Watson, T.W. Keal, P. Sherwood, A. Walsh, A.A. Sokol, *Nat. Mater.* 12 (2013) 798.

[46] S.J. Hong, S. Lee, J.S. Jang, J.S. Lee, *Energy Environ. Sci.* 4 (2011) 1781–1787.

[47] K.T. Butler, B.J. Dringoli, L. Zhou, P.M. Rao, A. Walsh, L.V. Titova, *J. Mater. Chem. A* 4 (2016) 18516–18523.

[48] A.J.E. Rettie, W.D. Chemelewski, D. Emin, C.B. Mullins, *J. Phys. Chem. Lett.* 7 (2016) 471–479.

[49] J. Wu, Y. Huang, W. Ye, Y. Li, *Adv. Sci.* 4 (2017) 1700194.

[50] E. Golias, M. Krivenkov, A. Varykhalov, J. Sánchez-Barriga, O. Rader, *Nano Lett.* 18 (2018) 3384–3390.

[51] M. Xie, Y. Feng, X. Fu, P. Luan, L. Jing, *J. Alloy. Compd.* 631 (2015) 120–124.

[52] F. Reurings, F. Tuomisto, C.S. Gallinat, G. Koblmüller, J.S. Speck, *Appl. Phys. Lett.* 97 (2010) 251907.

[53] F. Chen, Q. Yang, J. Sun, F. Yao, S. Wang, Y. Wang, X. Wang, X. Li, C. Niu, D. Wang, G. Zeng, *ACS Appl. Mater. Interfaces* 8 (2016) 32887–32900.

[54] P. Luan, M. Xie, X. Fu, Y. Qu, X. Sun, L. Jing, *Phys. Chem. Chem. Phys.* 17 (2015) 5043–5050.

[55] X. Fu, M. Xie, P. Luan, L. Jing, *ACS Appl. Mater. Interfaces* 6 (2014) 18550–18557.